Resonance Raman Excitation Profile of a Ruthenium(II) Complex of Dipyrido[2,3-*a*:3′,2′-*c*]phenazine

Sarah L. Howell,[†] Keith C. Gordon,*[,†] Mark R. Waterland,[‡] King Hung Leung,[§] and David Lee Phillips[§]

Department of Chemistry, University of Otago, Union Place, Dunedin, New Zealand, Nanomaterials Research Centre, Massey University, Colombo Road, Palmerston North, New Zealand, and Department of Chemistry, The University of Hong Kong, Pokfulam Road, Hong Kong SAR, PR China

Received: May 24, 2006; In Final Form: August 2, 2006

The lowest energy transition of $[Ru(CN)_4(ppb)]^{2-}$ (ppb = dipyrido[2,3-*a*:3′,2′-*c*]phenazine), a metal-to-ligand charge transfer, has been probed using resonance Raman spectroscopy with excitation wavelengths (488, 514, 530, and 568 nm) spanning the lowest energy absorption band centered at 522 nm. Wave packet modeling was used to simultaneously model this lowest energy absorption band and the cross sections of the resonance Raman bands at the series of excitation wavelengths across this absorption band. A fit to within ±20% was obtained for the Raman cross sections, close to the experimental uncertainty which is typically 10−20%. Δ values of 0.1−0.4 were obtained for modes which were either localized on the ppb ligand (345−1599 cm^{-1}) or the CN modes (2063 and 2097 cm^{-1}). DFT calculations reveal that the resonance Raman bands observed are due to modes delocalized over the entire ppb ligand.

Introduction

Inorganic complexes containing polypyridyl ligands show promise in a number of applications including solar energy systems[1−5] and as dopants in organic-based light-emitting diodes.[6−12] In these applications the excited state is the functional state and photophysical properties such as the excited-state lifetime are important. In many metal polypyridyl complexes the key excited state is the metal-to-ligand charge-transfer (MLCT) state,[13] and for such states the excited-state lifetime is dictated by both the energy gap law and the structural changes that occur upon excitation.[14−17] In general, the rate of nonradiative deactivation of the excited state is increased as the energy of the state lowers, the energy gap law.[14] However, it has been recognized that creating MLCT states that are delocalized can reduce nonradiative deactivation rates and thus increase excited-state lifetimes even in systems with low-lying excited states. One example of systems that accomplish this are complexes containing dipyrido[2,3-*a*:3′,2′-*c*]phenazine (ppb) (Figure 1) and substituted analogues. Treadway et al. reported the excited-state lifetime of $[Ru(bpy)_2(ppb)]^{2+}$ as 327 ns.[18] Gordon et al. investigated substituted analogues and found the excited-state lifetimes of $[Ru(bpy)_2(ppbCl_2)]^{2+}$ and $[Ru(bpy)_2(ppbMe_2)]^{2+}$ to be 124 and 600 ns, respectively.[19] Therefore, determining the extent of structural change is an important requirement in understanding excited-state properties.

Resonance Raman spectroscopy is the ideal probe of the initially photoexcited Franck−Condon state. Resonance Raman spectroscopy causes a 10^3-10^5 times enhancement in intensities compared to the normal Raman spectrum.[20,21] Importantly, this enhancement effect is selective, with only some of the bands being enhanced in intensity. As a general rule, one of the requirements for resonant enhancement is that the mode must be totally symmetric, in the point group common to both the ground- and excited-state geometry. The other requirement is that the mode must distort the molecular geometry of the ground state in such a way that it mimics the excited-state geometry.[20,21]

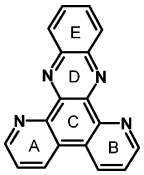

Figure 1. Structure of ppb with ring labeling shown.

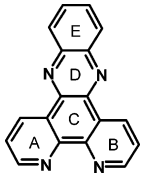

Figure 2. Dppz with ring labeling shown.

This enhancement effect may be used qualitatively to determine an excited-state structure. Resonance Raman spectroscopy was used by Gordon et al. to determine the nature of the Franck−Condon state for Cu(I) and Re(I) complexes of a series of substituted dipyrido[3,2-*a*:2′,3′-*c*]phenazine (dppz) ligands (Figure 2), an isomer of ppb.[22] Dppz complexes are of interest to study as, among other reasons, the nature of their excited state can be tuned by varying the nature of the metal moiety and substituents on the dppz ligand.[23,24] Dppz and substituted analogues have close-lying unoccupied molecular orbitals. For dppz the lowest energy unoccupied molecular orbital is localized on the phenazine portion (rings C−E; see Figure 2 for ring assignments) of the dppz and has b_1 symmetry. The two higher unoccupied molecular orbitals are localized on the phen (rings A−C) (b_1 symmetry) and phenazine (a_2 symmetry) portions.[25]

* To whom correspondence should be addressed. E-mail: kgordon@chemistry.otago.ac.nz.
[†] University of Otago.
[‡] Massey University.
[§] The University of Hong Kong.

10.1021/jp063197b CCC: $33.50
Published on Web 09/06/2006

In metal complexes of dppz it had been proposed that the Franck−Condon state is MLCT in nature and has an electron populating the molecular orbital localized on the phen portion and this then leads to rapid reorganization to an MLCT state where the b_1(phenazine) orbital is populated.[25] In the resonance Raman spectrum of $[Re(CO)_3Cl(dppz)]$ a number of bands were seen at 1315, 1406, 1446, 1473, and 1495 cm^{-1}. Density functional theory calculations were used to aid the interpretation of the resonance Raman spectra collected by Gordon et al.[24,26] Most of these bands are due to phen-based modes, with one being a delocalized mode and another is a phenazine-based mode. The dominance of phen-based over phenazine-based modes supports that the molecular orbital initially populated upon excitation is phen-based. The prevalence of phen-based modes was also observed for $[Cu(dppz)(PPh_3)_2]^+$ and Re(I) complexes of a variety of dppz-type ligands substituted with CH_3 and OCH_3 groups.

RREP can provide a quantitative description of the distorted excited-state geometry. Numerous studies have been carried out by Kelley and her research group on intra- and intermolecular charge-transfer complexes.[27−32] Although 2^N possible geometry changes are consistent with the resonance Raman intensities, where N is the number of active vibrational modes, the excited-state geometry may be still be obtained.[33]

It has been found that the $[Ru(CN)_4(L)]^{2-}$ analogues (where L = ppb and its analogues) have short MLCT excited states in water (<5 ns);[19] however, these complexes are advantageous for RREP modeling. First, the $[Ru(CN)_4(L)]^{2-}$ type complexes contain MLCT transitions which terminate on the L ligand, whereas the commonly studied $[Ru(bpy)_2(L)]^{2+}$ complexes may have overlapping Ru → L and Ru → bpy transitions each contributing to the observed resonance Raman spectrum. Thus, the observed resonance Raman spectra for the $[Ru(CN)_4(L)]^{2-}$ complexes are easier to interpret. Second, the CN vibrations offer a probe of the perturbation of the metal dπ configuration in the resonant MLCT transition.

Methods

Synthesis. The synthesis of ppb has been previously reported;[34] the complexes were synthesized using an adaptation of the method reported by Bignozzi et al.[35]

$Na_2[Ru(CN)_4(ppb)]$. $Na_4[Ru(CN)_6]$ (270 mg, 0.89 mmol) in water (250 mL) was added to ppb (270 mg, 0.95 mmol) in methanol (250 mL). The resulting clear solution was thoroughly purged with argon in a quartz reaction vessel and irradiated with 254 nm light in a Rayonet reactor for 32 h. The now purple solution was concentrated and extracted 3 times with 50 mL of dichloromethane. The desired product was separated from unreacted $Na_4[Ru(CN)_6]$ and the binuclear product on a Sephadex DEAE-A25 column, the purple product eluting with 0.3 M NaI. The solution was concentrated and the product precipitated by slow addition to acetone. This was repeated to ensure no NaI remained. Yield: 57% (270 mg, 0.51 mmol). ^{1}H NMR (300 MHz, D_2O): δ 9.94 (d, J^d = 8.0 Hz, 1H), 9.60 (d, J^d = 4.0 Hz, 2H), 8.41 (d, J^d = 10.0 Hz, 1H) 8.22 (m, 3H), 8.03 (m, 2H), 7.66 (t, J^t = 8.0 Hz, 1H), 6.44(t, J^t = 7.0 Hz, 1H). ^{13}C NMR (500 MHz, D_2O): δ 164.7, 163.8, 163.3, 162.1, 154.3, 151.7, 148.1, 145.9, 145.8, 144.0, 143.7, 142.2, 134.5, 133.8, 133.2, 132.0, 131.7, 131.0, 128.9, 127.4, 125.5, 125.0. ES-MS: m/z 511 [{M − Na}$^-$], 489.

Physical Measurements. Spectroscopic grade solvents were used for all spectroscopic measurements.

Spectral data was analyzed using Galactic Industries GRAMS/32 AI software.

^{1}H NMR spectra were recorded at 25 °C, using either a Varian 300 MHz NMR spectrometer. Chemical shifts are given relative to residual solvent peaks. Mass spectrometry measurements were obtained from a Micromass LCT instrument for electrospray measurements.

Continuous-wave Innova I-302 krypton-ion (Coherent, Inc.) and Spectra-Physics model 166 argon-ion lasers were used to generate resonance Raman scattering. The laser output was adjusted to give 20 mW at the sample, which was monitored using a Melles Griot 13 PEM 003 30-W broad-band power/energy meter. The incident beam and the collection lens were arranged in a 135° backscattering geometry to reduce Raman intensity reduction by self-absorption.[36] An aperture-matched lens was used to focus scattered light through a narrow band line-rejection (notch) filter (Kaiser Optical Systems) and a quartz wedge (Spex) and onto the 100 μm entrance slit of a spectrograph (Acton Research SpectraPro 500i). The collected light was dispersed in the horizontal plane by a 1200 grooves/mm ruled diffraction grating (blaze wavelength 500 nm) and detected by a liquid-nitrogen-cooled back-illuminated Spec-10:100B CCD controlled by a ST-133 controller and WinSpec/32 (version 2.5.8.1) software (Roper Scientific). Wavenumber calibration was performed using Raman bands from a 1:1 (by volume) mixture of acetonitrile and toluene sample.[37,38] Peak positions were reproducible to within 1−2 cm^{-1}. Spectra were obtained with a resolution of 5 cm^{-1}. Freshly prepared samples were held in a spinning NMR tube. Concentrations used were 0.1 mmol dm^{-3}.

Electronic absorption spectra were recorded on a Varian Cary 500 scan UV−vis−NIR Spectrophotometer, with Cary WinUV software. Samples were 10^{-4} mol dm^{-3}.

Quantum Chemical Calculations. The geometry, vibrational frequencies, and their IR and Raman intensities were calculated using DFT calculations (B3LYP functional) with the basis sets 6-31G(d) and LANL2DZ (on Ru atoms). These were implemented with the Gaussian 03W[39] program package. No negative frequencies were predicted indicating that the structures obtained were at energy minima. The visualization of the vibrational modes was provided by GaussViewW (Gaussian Inc.). The calculations of ppb and ppb$^{\bullet-}$ have been previously reported,[40] as have those of $[Ru(CN)_4(ppb)]^{2-}$ and $[Ru(CN)_4(ppb)]^{2-*}$.[19] A scale factor of 0.973 has been used for all calculated frequencies of $[Ru(CN)_4(ppb)]^{2-}$ <1700 cm^{-1}. The simulated resonance Raman spectrum was created using Gaussian curves with a fwhm of 4 cm^{-1}.

Wave Packet Modeling. The resonance Raman spectra are corrected for the wavelength sensitivity of the spectrograph and detection system. In aqueous solutions the sulfate anion was used as an internal intensity standard. Band areas were integrated using the GRAMS AI software package, and differential cross sections were obtained by taking the ratio of the internal standard to the band of interest. The resonance Raman intensities were modeled using the time-dependent wave packet picture described below. In this description, the excited surface is modeled semiempirically with various approximations as described below. It is convenient to use a dimensionless displacement, Δ, to describe the multidimensional potential surfaces. Δ_i describes the dimensionless displacement along a normal mode, i. The Δ_i are related to changes in internal coordinates, S_j, via an orthogonal transformation matrix, R_{ij}.

The absorption spectra and the Raman data were modeled simultaneously using the same material parameters to provide a check on the quality of the fit to the Raman data.

Theory

A brief discussion of the theory behind RREP modeling is presented herein. For more detailed discussions, see articles

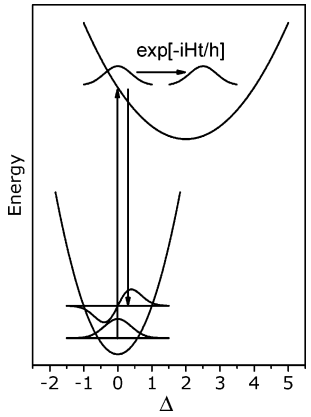

Figure 3. Time-domain picture of molecular spectroscopy. Wave packet dynamics on the excited-state surface determine a time-dependent overlap integral with the ground-state wave functions. For absorption the overlap integral involves the ground-state $n = 0$ vibrational wave function, and resonance Raman intensities are determined by the overlap with the $n = 1$ vibrational wave function.

by Myers.[41,42] The resonance Raman amplitudes are modeled using the semiempirical formalism developed by Heller and co-workers.[43]

The Raman amplitude between the initial and final vibrational states, α_{if}, is calculated as the half-Fourier transform of the time-dependent overlap of a wave packet propagating on the resonant electronic excited and the $v'' = 1$ ground-electronic-state vibrational wave function (Figure 3):

$$\alpha_{if}(\omega_L,\delta) = \frac{1}{\hbar}\int_0^\infty dt\langle\chi_f|\chi_i(t)\rangle \exp[i(\omega_L - \omega - \delta + \omega_i)t - g(t)]$$

Here ω_L is the incident laser frequency, $\hbar\omega_i$ is the energy of the initial vibrational level (set to zero as scattering from all modes in the simulation occurs from the ground vibrational level), ω is the zero−zero electronic transition frequency, and δ is the electronic zero−zero frequency shift due to inhomogeneous broadening. $\langle\chi_f| = \langle f|\mu_0$ and $\langle\chi_i| = \langle i|\mu_0$ are the multidimensional ground-state vibrational wave functions multiplied by the transition dipole moment, and $|\chi_i(t)\rangle = \exp(-iHt/\hbar)|\chi_i\rangle$ is the initial vibrational wave function propagated for a time, t, on the electronic excited-state surface, by the excited-state vibrational Hamiltonian. $g(t)$ is the solvent-broadening function modeled as an overdamped Brownian oscillator.[44] Separable harmonic oscillators, with frequencies taken from the ground-state Raman modes, were used in the model for the potential energy surfaces. The ground- and excited-state normal modes are assumed to have the same form; i.e., Dushinsky rotation is not included, and non-Condon effects were not included.

The experimental observable, the differential Raman cross section, is calculated via

$$\left(\frac{d\sigma}{d\Omega}\right)_{\parallel+\perp} = \sum_i B_i \sum_f \int d\omega_s \left(\frac{\omega_S{}^3\omega_L}{c^4}\int_{-\infty}^{+\infty} d\delta G(\delta)\left|\alpha_{if}(\omega_L,\delta)\right|^2\right) L_{if}(\omega_L - \omega_S)$$

where B_i is the Boltzmann population of the initial vibrational state (assumed to be unity here) and $L_{if}(\omega_L - \omega_S)$ is a Raman line-shape function. $G(\delta)$ is a normalized inhomogeneous broadening function which is taken to be Gaussian.

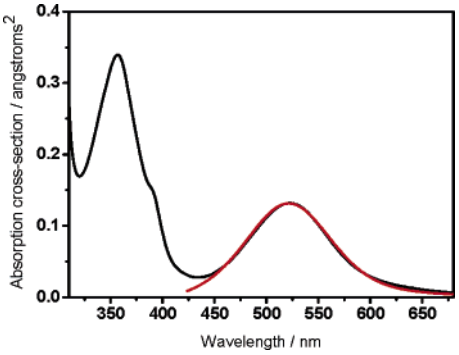

Figure 4. Measured (black) and simulated (red) electronic absorption spectrum of $[Ru(CN)_4(ppb)]^{2-}$.

The absorption cross section is calculated at the same level of theory using

$$\sigma_A(\omega) = \frac{4\pi|\mu|^2\omega}{3n\hbar c}\sum_i B_i\int_{-\infty}^{+\infty} d\delta G(\delta)\mathrm{Re}\int_{-\infty}^{+\infty} dt\langle\chi_i|\chi_i(t)\rangle \exp[i(\omega_L - \omega - \delta + \omega_i)t - g(t)]$$

where the real part of the Fourier transform is taken and n is the refractive index of the solvent.

Results and Discussion

DFT Calculations. The B3LYP/6-31G(d) calculations of the structure and vibrational spectra of $[Ru(CN)_4(ppb)]^{2-}$ have been previously reported.[19] The band assignments from that paper will be used in this discussion. The mean absolute deviation between calculated and measured vibrational frequencies was found to be 9 cm^{-1} for IR and Raman bands in the 1000−1650 cm^{-1} region.

Electronic Absorption Spectrum. The electronic spectrum of $[Ru(CN)_4(ppb)]^{2-}$ has an MLCT band centered at 522 nm (Figure 4). It is this band that has been fitted using RREP. This band is well isolated from any other transitions which allows for a single state model to be used. In cases where there are two or more overlapping transitions a multistate model is required.[45] The excitation wavelengths used to collect the resonance Raman spectra were 488, 514, 530, and 568 nm.

Resonance Raman Spectra and Simulations. The resonance Raman spectra of $[Ru(CN)_4(ppb)]^{2-}$ have a large number of bands (>50; Figure S1, Supporting Information); however, to simplify the modeling we have limited the analysis to 30 modes. The bands expected to have the smallest contribution have been excluded from the analysis. The resonance Raman bands considered and their absolute Δ values are tabulated in Table 1.

The simulated fit to the lowest energy metal-to ligand charge-transfer band in the absorption spectrum of $[Ru(CN)_4(ppb)]^{2-}$ is shown in Figure 4. A good fit has been obtained with the wave packet modeling with a single excited state suggesting the parameters obtained are a reasonable model of what happens upon photoexcitation of the complex.

The simulated resonance Raman spectrum (from the wave packet modeling) of $[Ru(CN)_4(ppb)]^{2-}$, along with the measured spectrum (both with 514.5 nm excitation), is shown in Figure 5. Although some bands differ slightly in intensity between the simulated and measured spectrum, overall the spectra are similar. The mean percentage deviation between the simulated and experimental intensities at this excitation wavelength is 20%. This compares well to the experimental uncertainty in the measurements which is typically 10−20%.[46]

TABLE 1: Wavenumbers of the Bands in the Resonance Raman Spectra of $[Ru(CN)_4(ppb)]^{2-}$, Along with the Calculated Absolute Δ Values and the DFT Calculated Vibrational Frequencies

ν/cm^{-1} expt	Δ	ν/cm^{-1} calcd	ν/cm^{-1} expt	Δ	ν/cm^{-1} calcd
345	0.3	343	1330	0.2	1320
356	0.4	344	1343	0.3	1344
491	0.3	471	1368	0.1	1354
574	0.2	580	1372	0.1	1395
588	0.2	589	1427	0.2	1398
629	0.2	612	1441	0.2	1448
639	0.2	641	1471	0.2	1476
659	0.2	690	1488	0.1	1486
722	0.2	700	1503	0.1	1500
780	0.2	763	1525	0.2	1541
1018	0.1	1024	1547	0.1	1555
1109	0.1	1090	1573	0.2	1576
1157	0.1	1151	1599	0.1	1578
1222	0.1	1226	2063	0.2	
1263	0.3	1257	2097	0.2	

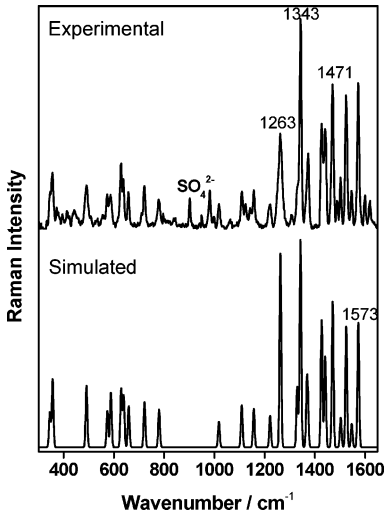

Figure 5. Measured and simulated resonance Raman spectrum of $[Ru(CN)_4(ppb)]^{2-}$ (λ_{ex} = 514.5 nm).

Selected resonance Raman profiles for $[Ru(CN)_4(ppb)]^{2-}$ are shown in Figure 6. These are the bands observed at 1263, 1471, 1573, and 2097 cm^{-1}. The Raman profiles largely follow the absorption band profile. This is expected for the case of a single electronic state contributing to the Raman scattering amplitude, as there are no interference effects that can lead to dips or increases in the Raman scattering amplitude.[47] Simultaneous motion along multiple vibrational modes leads to rapid depletion of the wave packet amplitude in the Franck−Condon region, and in this case the mode profiles are sensitive to the magnitude of the dimensionless displacements (Δ's). All the modes in Table 1 have very similar displacements, leading to very similar band shapes for the Raman profiles. The absorption maximum occurs at 522 nm. The excitation wavelength for which the largest cross section occurs is 514 nm, close to this absorption maximum. All three bands show a reasonable agreement between observed and calculated cross sections.

In the <1000 cm^{-1} region of the spectrum, the bands with the greatest absolute Δ values are at 345, 356, and 491 cm^{-1}. These bands have Δ values of 0.3−0.4. These bands are predicted to be modes of a_1 symmetry occurring at 343, 344, and 471 cm^{-1}, respectively. These modes are predominately motion of atoms in ring C of the ppb ligand (see Figure 1 for ring labels) along with a small amount of contribution from ring D and the CN ligands.

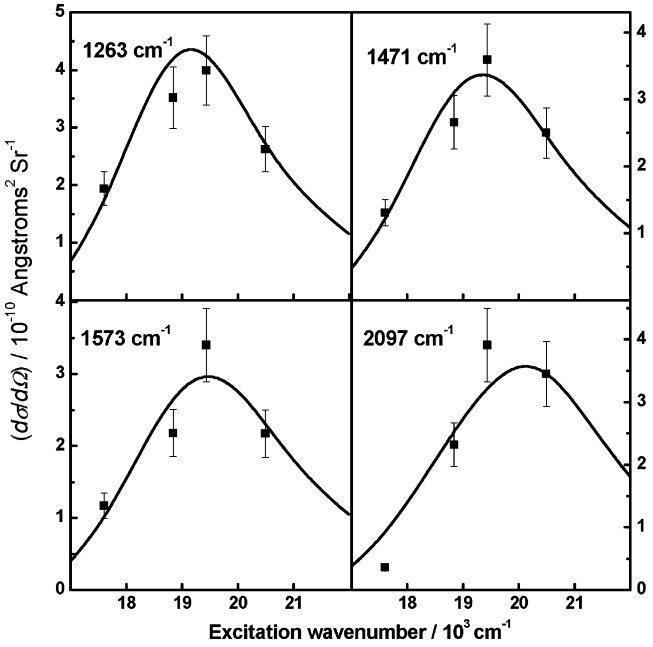

Figure 6. Selected resonance Raman excitation profiles of $[Ru(CN)_4(ppb)]^{2-}$. The points are the experimental data (with 15% error bars), and the lines are the simulated excitation profiles.

In the 1000−1650 cm^{-1} region of the spectrum, bands at 1263, 1343, and 1471 cm^{-1} have the largest absolute Δ values at 0.3 each. These bands correspond to modes calculated at 1257, 1344, and 1476 cm^{-1}. These are all modes of a_1 symmetry assuming C_{2v} symmetry of the ppb ligand. All three of these vibrational modes are delocalized over all 5 rings of the ppb ligand.

One of the most intense bands in the resonance Raman spectra is due to a CN modes of the complex and is observed at 2097 cm^{-1}. A second CN band is observed at 2063 cm^{-1}. The enhancement of these modes is consistent with the transition to an MLCT excited state. The decrease in electron density at the ruthenium center can be approximately described as the oxidation of Ru(II) to Ru(III). This is accompanied by a decrease in back-bonding to the CN ligands and hence a decrease in the population of the π^* orbitals on these ancillary ligands. This causes a shortening of the C−N bond. It is this excited-state structural change which causes resonant enhancement. The wave packet modeling of these CN bands at 2063 and 2097 cm^{-1} shows reasonable agreement with the absolute cross sections that were observed. The excitation profile of the 2097 cm^{-1} band can be seen in Figure 6. There are a total of four CN modes observed in the normal Raman spectrum of $[Ru(CN)_4(ppb)]^{2-}$; these lie at 2045, 2063, 2097, and 2108 cm^{-1} (Figure S2). The only two bands that show intensity in the resonance Raman spectrum are those at 2063 and 2097 cm^{-1}, with the latter being much more strongly enhanced. Comparison of these bands to the modes calculated using DFT methods reveals that the band at 2063 cm^{-1} is almost exclusively the antisymmetric stretch of the axial CN ligands, while the band at 2097 decrease bonding to each of the equatorial CN's (Figure S3). The effect of the MLCT transition is to depopulate a dπ molecular orbital which in turn alters the level of back-bonding to the CN ligand, mitigated by polypyridyl radical anion back-bonding.[48−50] An examination of the dπ orbitals involved shows that their symmetry is such that they act to decrease bonding to each of the equatorial CN ligands (Figure S4). It is therefore intuitive to observe increased enhancement from the mode that is symmetric in the equatorial CN stretch (2097 cm^{-1} band) and less enhancement from the axial vibration (2063 cm^{-1} band).

The ligand vibrational modes observed in the resonance Raman spectra are typically delocalized over the entire ppb ligand, in contrast to the closely related dppz ligands whose complexes typically show localized dppz vibrational modes.[22,51−53] This suggests that, unlike for dppz complexes, the structural changes upon excitation of this ppb complex are spread over the entire ppb ligand. This is consistent with the DFT calculated triplet-state structure of $[Ru(CN)_4(ppb)]^{2-}$ which predict bond lengths of the ppb ligand remain within 0.01 Å of the ground-state structure.[19]

Two recent RREP studies on polypyridyl complexes were carried out by McHale et al.[54] on $[Ru(bpy)(NH_3)_4]^{2-}$ and by Waterland et al.[46] on $[Cu(pqx)(PPh_3)_2]^+$ (pqx = 2-(2′-pyridyl)-quinoxaline). McHale et al. determined the Δ values of $[Ru(bpy)(NH_3)_4]^{2-}$ in both methanol and DMSO. The lowest energy band in the electronic absorption spectrum of $[Ru(bpy)(NH_3)_4]^{2-}$ comprises two overlapping MLCT bands. Thus, the resonance Raman and electronic absorption bands were modeled using two states. The Δ values obtained were found to be between 0.03 and 0.20 for both solvents. Little variation was found between the Δ values in different solvents. No resonance Raman bands were observed for the NH_3 modes. Unlike the CN ligands of $[Ru(CN)_4(ppb)]^{2-}$, the NH_3 ligand vibrations are not strongly coupled to the MLCT transition; hence, NH_3 modes do not exhibit resonance enhancement upon excitation into the MLCT excited state. The Δ values for $[Ru(bpy)(NH_3)_4]^{2-}$ had been reported by Hupp et al. in 1989.[55] The Δ values were found to be up to 1 order of magnitude greater than those determined by McHale et al., but Hupp et al. had not accounted for solvent reorganization, which McHale et al. suggest has a larger contribution than internal reorganization, nor had they recognized that there were two overlapping transitions giving rise to the lowest energy electronic absorption band. Hence, the Δ values determined by Hupp et al. may have been overestimated.

The study by Waterland et al.[46] on $[Cu(pqx)(PPh_3)_2]^+$ found that the lowest energy MLCT band at 431 nm overlaps with a ligand-centered transition band at 328 nm. These overlapping bands necessitated the use of a two state model. The Δ values were determined in dichloromethane and chloroform. The values were found to be the same between the two solvents. The largest Δ value was for the mode at 538 cm^{-1} (Δ = 1.5−1.7). The mode at 538 cm^{-1} comprises significant distortion about the Cu center. This is consistent with the change in geometry of the tetrahedral Cu(I) center upon oxidation in the MLCT excited state to Cu(II) which is 5 or 6 coordinate. Such reorganization is not expected for the Ru(II) to Ru(III) in the $[Ru(CN)_4(ppb)]^{2-}$ complex; hence, no resonance enhancement is observed for modes associated with the metal center. The ligand-based modes of $[Cu(pqx)(PPh_3)_2]^+$ typically had Δ values of 0.2−0.5, slightly larger than those of $[Ru(CN)_4(ppb)]^{2-}$.

The transition dipole length for the MLCT transition was found to be 0.63 Å. This is close to the values of 0.625 and 0.650 Å found for the MLCT state of $[Cu(pqx)(PPh_3)_2]^+$ in dichloromethane and chloroform, respectively.[46] As previously discussed by Waterland et al., the short transition dipole length is consistent with an intramolecular charge transfer.[46]

Conclusions

A single-state wave packet model has been used to gain insight into the structure of the Franck−Condon MLCT excited state of $[Ru(CN)_4(ppb)]^{2-}$. A large number of ppb bands undergo resonant enhancement between 345 and 1599 cm^{-1}, as well as bands due to the CN ligands, supporting the assignment of a MLCT excited state. The Δ values determined by the simultaneous fitting of the absorption and Raman spectra suggest that the structural changes that occur upon excitation to the MLCT state are modest. DFT calculations predict that the vibrational modes are delocalized over the entire ppb ligand, which in turn implies that the structural changes upon excitation are also delocalized.

Acknowledgment. The following are thanked: Dr. Matthew Polson for providing the complex used in this study; the University of Otago and the MacDiarmid Institute for Advanced Materials and Nanotechnology for supporting this research. S.L.H. thanks the Foundation of Research, Science, and Technology for funding.

Supporting Information Available: Figures showing resonance Raman spectra of $[Ru(CN)_4(ppb)]^{2-}$ in 0.1 M Na_2SO_4(aq), the FT-Raman spectrum of $[Ru(CN)_4(ppb)]^{2-}$ in water, eigenvectors of the vibrational modes responsible for the two CN bands in the resonance Raman spectra of $[Ru(CN)_4(ppb)]^{2-}$, and MO diagrams of $[Ru(CN)_4(ppb)]^{2-}$. This material is available free of charge via the Internet at http://pubs.acs.org.

References and Notes

(1) Bach, U.; Lupo, D.; Comte, P.; Moser, J. E.; Weissortel, F.; Salbeck, J.; Spreitzer, H.; Gratzel, M. *Nature* **1998**, *395*, 583.

(2) Nazeeruddin, M. K.; Graetzel, M. Conversion and storage of solar energy using dye-sensitized nanocrystalline TiO2 cells. In *Comprehensive Coordination Chemistry II*; Ward, M. D., Ed.; Elsevier Ltd.: Oxford, U.K., 2004; Vol. 9; p 719.

(3) Nazeeruddin, M. K.; Klein, C.; Liska, P.; Graetzel, M. *Coord. Chem. Rev.* **2005**, *249*, 1460.

(4) Pollard, J. A.; Zhang, D.; Downing, J. A.; Knorr, F. J.; McHale, J. L. *J. Phys. Chem. A* **2005**, *109*, 11443.

(5) Wang, P.; Klein, C.; Moser, J.-E.; Humphry-Baker, R.; Cevey-Ha, N.-L.; Charvet, R.; Comte, P.; Zakeeruddin, S. M.; Graetzel, M. *J. Phys. Chem. B* **2004**, *108*, 17553.

(6) Kavitha, J.; Chang, S.-Y.; Chi, Y.; Yu, J.-K.; Hu, Y.-H.; Chou, P.-T.; Peng, S.-M.; Lee, G.-H.; Tao, Y.-T.; Chien, C.-H.; Carty, A. J. *Adv. Funct. Mater.* **2005**, *15*, 223.

(7) Chen, Y.-L.; Lee, S.-W.; Chi, Y.; Hwang, K.-C.; Kumar, S. B.; Hu, Y.-H.; Cheng, Y.-M.; Chou, P.-T.; Peng, S.-M.; Lee, G.-H.; Yeh, S.-J.; Chen, C.-T. *Inorg. Chem.* **2005**, *44*, 4287.

(8) Holder, E.; Langeveld, B. M. W.; Schubert, U. S. *Adv. Mater.* **2005**, *17*, 1109.

(9) Yersin, H. *Top. Curr Chem.* **2004**, *241*, 1.

(10) Wang, J. F.; Jabbour, G. E.; Mash, E. A.; Anderson, J.; Zhang, Y.; Lee, P. A.; Armstrong, N. R.; Peyghambarian, N.; Kippelen, B. *Adv. Mater.* **1999**, *11*, 1266.

(11) Lamansky, S.; Djurovich, P.; Murphy, D.; Abdel-Razzaq, F.; Lee, H.-E.; Adachi, C.; Burrows, P. E.; Forrest, S. R.; Thompson, M. E. *J. Am. Chem. Soc.* **2001**, *123*, 4304.

(12) Carlson, B.; Phelan, G. D.; Kaminsky, W.; Dalton, L.; Jiang, X.; Liu, S.; Jen, A. K. Y. *J. Am. Chem. Soc.* **2002**, *124*, 14162.

(13) Kalyanasundaram, K. *Photochemistry of Polypyridine and Porphyrin Complexes*; Academic Press: San Diego, CA, 1992.

(14) Caspar, J. V.; Kober, E. M.; Sullivan, B. P.; Meyer, T. J. *J. Am. Chem. Soc.* **1982**, *104*, 630.

(15) McClanahan, S. F.; Dallinger, R. F.; Holler, F. J.; Kincaid, J. R. *J. Am. Chem. Soc.* **1985**, *107*, 4853.

(16) Whittle, C. E.; Weinstein, J. A.; George, M. W.; Schanze, K. S. *Inorg. Chem.* **2001**, *40*, 4053.

(17) Yoblinski, B. J.; Stathis, M.; Guarr, T. F. *Inorg. Chem.* **1992**, *31*, 5.

(18) Treadway, J. A.; Loeb, B.; Lopez, R.; Anderson, P. A.; Keene, F. R.; Meyer, T. J. *Inorg. Chem.* **1996**, *35*, 2242.

(19) Howell, S. L.; Gordon, K. C.; McGarvey, J. J. *J. Phys. Chem. A* **2005**, *109*, 2948.

(20) Clark, R. J. H.; Dines, T. J. *Angew. Chem.* **1986**, *98*, 131.

(21) Hirakawa, A. Y.; Tsuboi, M. *Science* **1975**, *188*, 359.

(22) Waterland, M. R.; Gordon, K. C. *J. Raman Spectrosc.* **2000**, *31*, 243.

(23) Kuimova, M. K.; Alsindi, W. Z.; Dyer, J.; Grills, D. C.; Jina, O. S.; Matousek, P.; Parker, A. W.; Portius, P.; Sun, X. Z.; Towrie, M.; Wilson, C.; Yang, J.; George, M. W. *Dalton Trans.* **2003**, 3996.

(24) Waterland, M. R.; Gordon, K. C.; McGarvey, J. J.; Jayaweera, P. M. *J. Chem. Soc., Dalton Trans.* **1998**, 609.

(25) Fees, J.; Kaim, W.; Moscherosch, M.; Matheis, W.; Klima, J.; Krejcik, M.; Zalis, S. *Inorg. Chem.* **1993**, *32*, 166.

(26) Waterland, M. R.; Gordon, K. C. *Laser Chem.* **1999**, *19*, 287.
(27) Kulinowski, K.; Gould, I. R.; Myers, A. B. *J. Phys. Chem.* **1995**, *99*, 9017.
(28) Markel, F.; Ferris, N. S.; Gould, I. R.; Myers, A. B. *J. Am. Chem. Soc.* **1992**, *114*, 6208.
(29) Moran, A. M.; Bartholomew, G. P.; Bazan, G. C.; Kelley, A. M. *J. Phys. Chem. A* **2002**, *106*, 4928.
(30) Moran, A. M.; Myers Kelley, A.; Tretiak, S. *Chem. Phys. Lett.* **2002**, *367*, 293.
(31) Moran, A. M.; Egolf, D. S.; Blanchard-Desce, M.; Kelley, A. M. *J. Chem. Phys.* **2002**, *116*, 2542.
(32) Moran, A. M.; Aravindan, P.; Spears, K. G. *J. Phys. Chem. A* **2005**, *109*, 1795.
(33) Lilichenko, M.; Tittelbach-Helmrich, D.; Verhoeven, J. W.; Gould, I. R.; Myers, A. B. *J. Chem. Phys.* **1998**, *109*, 10958.
(34) Polson, M. I. J.; Howell, S. L.; Flood, A.; Blackman, A. G.; Gordon, K. C. *Polyhedron* **2004**, *23*, 1427.
(35) Bignozzi, C. A.; Chiorboli, C.; Indelli, M. T.; Rampi Scandola, M. A.; Varani, G.; Scandola, F. *J. Am. Chem. Soc.* **1986**, *108*, 7872.
(36) Shriver, D. F.; Dunn, J. B. R. *Appl. Spectrosc.* **1974**, *28*, 319.
(37) McCreery, R. L. *Raman Spectroscopy for Chemical Analysis*; John Wiley & Sons: New York, 2000.
(38) The ASTM subcommitte on Raman spectroscopy has adopted eight materials as Raman shift standards (ASTM E 1840). The band wavenumbers for these standards are available at: http://chemistry.ohio-state.edu/~rmccreer/shift.html.
(39) Frisch, M. J.; G. W. T.; Schlegel, H. B.; Scuseria, G. E.; Robb, M. A.; Cheeseman, J. R.; Montgomery, J. A., Jr.; Vreven, T.; Kudin, K. N.; Burant, J. C.; Millam, J. M.; Iyengar, S. S.; Tomasi, J.; Barone, V.; Mennucci, B.; Cossi, M.; Scalmani, G.; Rega, N.; Petersson, G. A.; Hada, H. N., M.; Ehara, M.; Toyota, K.; Fukuda, R.; Hasegawa, J.; Ishida, M.; Nakajima, T.; Honda, Y.; Kitao, O.; Nakai, H.; Klene, M.; Li, X.; Knox, J. E.; Hratchian, H. P.; Cross, J. B.; Adamo, C.; Jaramillo, J.; Gomperts, R.; Stratmann, R. E.; Yazyev, O.; Austin, A. J.; Cammi, R.; Pomelli, C.; Ochterski, J. W.; Ayala, P. Y.; Morokuma, K.; Voth, G. A.; Salvador, P.; Dannenberg, J. J.; Zakrzewski, V. G.; Dapprich, S.; Daniels, A. D.; Strain, M. C.; Farkas, O.; Malick, D. K.; Rabuck, A. D.; Raghavachari, K.; Foresman, J. B.; Ortiz, J. V.; Cui, Q.; Baboul, A. G.; Clifford, S.; Cioslowski, J.; Stefanov, B. B.; Liu, G.; Liashenko, A.; Piskorz, P.; Komaromi, I.; Martin, R. L.; Fox, D. J.; Keith, T.; Al-Laham, M. A.; Peng, C. Y.; Nanayakkara, A.; Challacombe, M.; Gill, P. M. W.; Johnson, B.; Wong, W. C., M. W.; Gonzalez, C.; Pople, J. A. *Gaussian 03*; Gaussian, Inc.: Pittsburgh, PA, 2003.
(40) Howell, S. L.; Matthewson, B. J.; Polson, M. I. J.; Burrell, A. K.; Gordon, K. C. *Inorg. Chem.* **2004**, *43*, 2876.
(41) Myers, A. B.; Hochstrasser, R. M. *J. Chem. Phys.* **1987**, *87*, 2116.
(42) Myers, A. B. *Excited Electronic State Properties from Ground-State Resonance Raman Intensities*; John Wiley & Sons: New York, 1995; Vol. 23.
(43) Heller, E. J. *Acc. Chem. Res.* **1981**, *14*, 368.
(44) Li, B.; Johnson, A. E.; Mukamel, S.; Myers, A. B. *J. Am. Chem. Soc.* **1994**, *116*, 11039.
(45) Egolf, D. S.; Waterland, M. R.; Kelley, A. M. *J. Phys. Chem. B* **2000**, *104*, 10727.
(46) Waterland, M. R.; Howell, S. L.; Gordon, K. C.; Burrell, A. K. *J. Phys. Chem. A* **2005**, *109*, 8826.
(47) Shin, K. S.; Zink, J. I. *J. Am. Chem. Soc.* **1990**, *112*, 7184.
(48) Dattelbaum, D. M.; Omberg, K. M.; Schoonover, J. R.; Martin, R. L.; Meyer, T. J. *Inorg. Chem.* **2002**, *41*, 6071.
(49) Dattelbaum, D. M.; Martin, R. L.; Schoonover, J. R.; Meyer, T. J. *J. Phys. Chem. A* **2004**, *108*, 3518.
(50) Dattelbaum, D. M.; Omberg, K. M.; Hay, P. J.; Gebhart, N. L.; Martin, R. L.; Schoonover, J. R.; Meyer, T. J. *J. Phys. Chem. A* **2004**, *108*, 3527.
(51) Lundin, N. J.; Walsh, P. J.; Howell, S. L.; McGarvey, J. J.; Blackman, A. G.; Gordon, K. C. *Inorg. Chem.* **2005**, *44*, 3551.
(52) Walsh, P. J.; Gordon, K. C.; Lundin, N. J.; Blackman, A. G. *J. Phys. Chem. A* **2005**, *109*, 5933.
(53) Matthewson, B. J.; Flood, A.; Polson, M. I. J.; Armstrong, C.; Phillips, D. L.; Gordon, K. C. *Bull. Chem. Soc. Jpn.* **2002**, *75*, 933.
(54) Streiff, J.; McHale, J. L. *J. Chem. Phys.* **2000**, *112*, 841.
(55) Doorn, S. K.; Hupp, J. T. *J. Am. Chem. Soc.* **1989**, *111*, 4704.